J Solid State Electrochem (2009) 13:887–893
DOI 10.1007/s10008-008-0623-2

ORIGINAL PAPER

Characterization and electrochemical applications of a carbon with high density of surface functional groups produced from beer yeast

Guo-Qing Zhang · Sheng-Tao Zhang

Received: 2 May 2008 / Revised: 26 June 2008 / Accepted: 29 June 2008 / Published online: 24 July 2008

Abstract Carbon materials enriched with nitrogen and oxygen surface functional groups were obtained by pyrolyzing strained beer yeast at 750 °C under an inert atmosphere. Physical and surface properties of the carbon obtained were characterized by X-ray powder diffraction, transmission electron microscopy, high-resolution transmission electron microscopy, Raman spectrometry, and X-ray photoelectron spectroscopy. Results show that the carbon possesses an amorphous structure, a spherical morphology, and a high density of surface functional groups. Electrochemical properties were evaluated by cyclic voltammetry, a galvanostatic charge–discharge technique, and electrochemical impedance spectroscopy. The carbon has 989.65 $mAh \cdot g^{-1}$ of initial discharge capacity and a stable cycle performance for a Li–C cell. A specific capacitance of 120 $F \cdot g^{-1}$ was obtained for a single carbon electrode and good cycle performance was achieved for a symmetrical supercapacitor fabricated using this carbon. These carbons derived from strained beer yeast have promising applications in energy storage and conversion systems.

Keywords Pyrolytic carbon · Electrochemical properties · Supercapacitor · Functional groups

G.-Q. Zhang · S.-T. Zhang (✉)
College of Chemistry and Chemical Engineering,
Chongqing University,
Chongqing 400030, People's Republic of China
e-mail: yzhanggq@163.com

G.-Q. Zhang
Department of Chemistry and Environment Science,
Yangtze Normal University,
Chongqing 408100, People's Republic of China

Introduction

The demands for advanced energy conversion and storage devices such as fuel cells, lithium-ion batteries, and supercapacitors have resulted in many recent studies on finding suitable advanced carbon materials. Various carbon materials, which differ in microstructure, morphology, particle size, pore size, and surface physicochemical characteristics, have distinct electrochemical properties for a wide range of applications, e.g., in sensors, energy storage and conversion systems, catalytic reactions, and absorption. It has been previously shown in many papers that surface functional groups (or complexes) anchored on or within carbon were responsible for the variety in physicochemical and catalytic properties of the material [1, 2]. Accordingly, how to modify and characterize surface functional groups to improve or extend practical applications of carbon was considered to be a subject of interest in this area.

Among many surface functional groups, the most common species on the surface of carbon contain oxygen and nitrogen. These significantly influence electrochemical performance of carbon. Some methods, such as mechanical [3], chemical [4], and electrochemical routes [5], have been successfully used to introduce oxygen-containing functional groups onto or into carbon. Various nitrogen-containing functional groups can be introduced by heating suitable polymeric precursors [6]. However, there are a few reports that both oxygen- and nitrogen-containing functional groups simultaneously exist on a carbon surface, and these species jointly contribute to the electrochemical behavior of carbon.

Waste products containing beer yeast can generally be used as an absorbing agent, drying agent, soil conditioner, catalyst, etc. To broaden industrial utilization of this kind of product, new research is necessary. In the present work, a

class of carbon with various surface functional groups was directly derived from carbonizing strained beer yeast for the first time. The suitability of the carbon obtained for a lithium-ion battery and supercapacitor was evaluated by using a series of electrochemical techniques. Experimental results are discussed in detail below.

Experimental

Heat treatment of strained beer lees (provided by HuangHe Beer Company, Lanzhou) was performed at 300 °C for 1 h then at 400 and 550 °C for 2 h, finally at 750 °C for 4 h in argon atmosphere. The resulting carbon was ground to a fine powder by ball-mill method and then activation was conducted using potassium hydroxide solution. The sample was mechanically mixed with fourfold amounts of 6-M potassium hydroxide solution (weight ratio, KOH solution–carbon=4) and then dried at 120 °C for 5 h under an inert argon flow of 500 ml·min^{-1}. The resulting activated product was cooled to room temperature and then washed repeatedly with deionized water to remove the potassium hydroxide until the pH of the filtrate reached approximately 7.

Physical and surface properties of the carbon obtained were characterized by X-ray powder diffraction (XRD, MAC Science M18XCE with Cu K_α radiation, Japan), transmission electron microscopy (TEM, Hitachi-600, Japan), high-resolution transmission electron microscopy (HRTEM, JEM-3000F, Japan), Raman spectrometry (Renishaw System with a 632.8 nm, 25 mW He–Ne laser, UMA), and X-ray photoelectron spectroscopy (XPS, V.G. ESCALab 2201-XL with Cu K_α radiation, UK).

Electrochemical characterization was carried out using a CHI 660A electrochemical workstation (CH Instruments, Cordova, TN, USA) and a galvanostatic charge–discharge unit (Arbin AT2042, College Station, TX, USA). Lithium–ion intercalation–deintercalation into or out the carbon was examined with the usual two-electrode system, which consisted of metallic lithium negative electrode and a carbon electrode (electrode area 2 cm^2) separated by a Celgard 2400 porous polypropylene film (Charlotte, NC, USA). The carbon electrode was made by mixing the carbon, acetylene black (AB), and polyvinylidene fluoride in a ratio of 80:15:5 by weight. The mixture was coated onto a copper disk sheet and then dried at 100 °C for 24 h in a vacuum oven before use. The electrolyte was 1 M $LiPF_6$ in ethylene carbonate and dimethyl carbonate (50:50 by volume). All cells were assembled in an argon-filled glove box. Capacitive characterization of the carbon was performed with a three-electrode system in which the carbon was used as positive electrode (0.2 cm^2, 6 mg), platinum foil as counter electrode, Hg–HgO electrode as reference electrode, and 6-M KOH solution as electrolyte. A symmetrical capacitor was fabricated with the carbon as electrodes. The carbon electrode was prepared according to the following steps. The mixture containing 80 wt.% carbon sample, 15 wt.% AB, and 5 wt.% polytetrafluoroethylene was well mixed and then pressed onto a nickel grid (1.2×10^7 Pa) that served as a current collector.

Results and discussion

XRD and Raman spectroscopy

XRD patterns of the carbon samples heat-treated at 300, 400, 550, and 750 °C were shown in Fig. 1. The patterns clearly change as temperature increases. The pattern at each

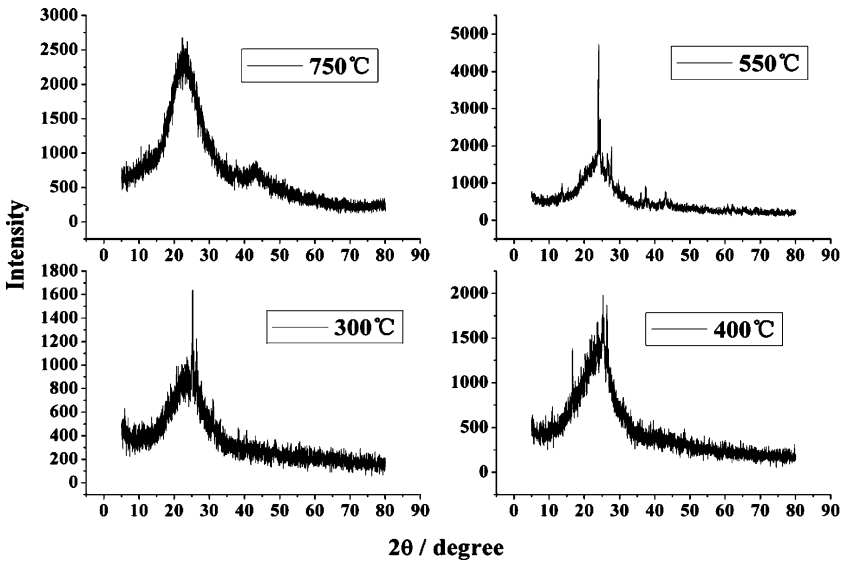

Fig. 1 XRD patterns for the carbon as a function of heat treatment temperature

Table 1 Structural parameters of the carbon

Temperature (°C)	(002) 2θ(°)	d_{002}/nm	L_c/nm	L_a/nm
300	25.60	0.357	1.083	2.215
400	25.44	0.359	1.028	2.103
550	23.82	0.383	1.026	2.096
750	23.55	0.388	1.025	2.095

temperature possesses a broad diffraction peak at around 25°, which can be assigned to the (002) crystal plane diffraction peak, showing presence of amorphous carbon and a low degree of graphitization. At 750 °C, a broad diffraction peak appears at 2θ angle of ~43°, which can be ascribed to convolution of the (10) hk bidimensional lines [7]. It has been reported by Inagaki [8] that the existence of hk lines resulted from turbostatic stacking of hexagonal layers reflects regularity along the *c*-axis, confirming the formation of a disordered carbon. The crystal structural parameters can be calculated by $L_{hkl} = k\lambda/\beta\cos\theta$ and $d_{002} = \lambda/2\sin\theta$. It can be seen from Table 1 that the (002) crystal plane diffraction angle shifts to a lower position with the rise of temperature. The corresponding crystal panel space (d_{002}) also increases gradually. These transformations illuminate that crystallinity and disordered nature of the carbon is enhanced as temperature increases. The broader width and lower position of the (002) crystal plane diffraction peak than that of graphite (d_{002}= 0.335 nm) indicate the low crystallinity of the carbon (d_{002}=0.356 nm, L_c=2.56 nm) [9]. The difference in the interlayer distances (d_{002}) between the carbon and graphite can be ascribed to some substitution of nitrogen atoms and arises from smaller diameter of nitrogen (1.50 Å) than that of carbon (1.54 Å) [10].

Its Raman spectrum may provide more convincing information about the crystallography of the carbon. For the first-order Raman scattering in Fig. 2, two bands at approximately 1,360 and 1,600 cm^{-1} may be analogs of the D- and G-bands of graphite, which are attributed to defect and disorder-induced mode, respectively [11]. The peak at 1,600 cm^{-1} is the G-band [12], attributed to vibration of sp^2-bonded carbon atom in a two-dimensional hexagonal lattice [13], namely, the stretching mode of the C=C bond of typical graphite. The peak at around 1,360 cm^{1} is the D-band associated with vibration of the carbon atom with a dangling bond in plane termination graphite and is also related to defects and disorder of carbon. It is worth noting that the peak positions of G- and D-band shift to a higher wavelength number in comparison with that of single crystal, suggesting a structural imperfection of the graphene sheets of material [14]. The relative intensity of the two peaks (I_G/I_D) is 0.99, and $\Delta\upsilon_G$ value (the full width at half-maximum (fwhm) of the G-band is 71 cm^{-1}, which is closely related to structural regularity [15]. The relative intensity ratio combined with high $\Delta\upsilon_G$ value reflects a low degree of graphitization of the carbon.

Morphology and XPS analysis

It can be seen from Fig. 3a that the carbon displays a perfectly bead-like shape and smooth particle surface. The diameter of individual particle is between 5 and 20 nm. In addition, the representative HRTEM image (Fig. 3b) shows clear lattice distance of approximately 3.56 Å that corresponds to the (002) crystal plane of the carbon.

XPS spectra of the carbon indicate the presence of three distinct peaks, which can be explained by existence of carbon, nitrogen, and oxygen atoms. Fitting of the C1 spectrum (Fig. 4a) can be resolved into five individual component peaks at binding energy of 281.6, 284.5, 288.4, 291.3, and 292.9 eV, representing carbidic carbon, graphitic carbon, carbonyl group, carboxyl or ester group, and shake-up satellite peak on account of n-rc* transition in aromatic rings or relative structure of C–N [16], respectively.

Fitted N1s regions indicate several different species present on the carbon surface (Fig. 4b). Nitrogen exists mainly in three states. Every individual component peak can be ascribed to pyridine-like structure [17] (398.7 eV),

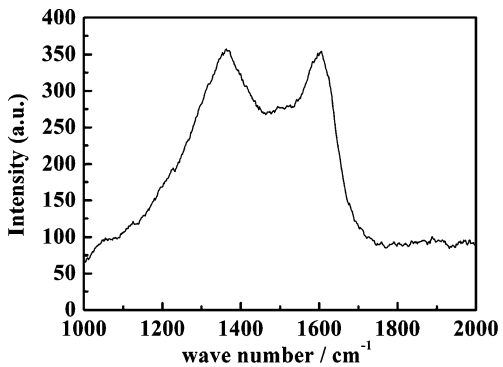

Fig. 2 Raman spectroscopy of the carbon

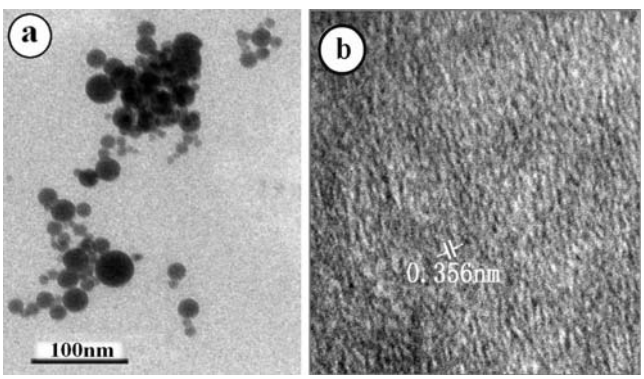

Fig. 3 TEM micrograph (**a**) and HRTEM image (**b**) of the carbon

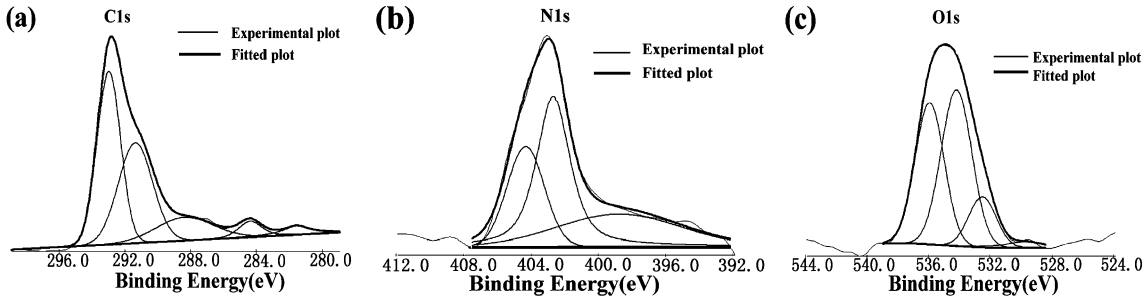

Fig. 4 X-ray photoelectron spectra of the carbon; **a** C1s, **b** N1s, and **c** O1s

pyridine-*N*-oxide (402.6 eV), and chemisorbed nitrogen oxide [18] (404.3 eV).

Various oxygen-containing functional groups existing on the carbon surface were also confirmed through XPS measurement (Fig. 4c). O1s core level spectrum reveals presence of four peaks, corresponding to C–O group (529.7 eV), C–OH and/or C–O–C group (532.5 eV), and chemisorbed oxygen and/or water (534.2, 535.6 eV) [19].

Electrochemical properties of the carbon for C–Li cell

It has been reported that many factors, such as morphology, surface area, and particle size, may significantly influence the electrochemical performance of carbon. The carbon obtained shows bead-like morphology and nanoscale particle size, with especially abundant surface functional groups existing on the carbon surface. Therefore, it was necessary to examine electrochemical properties of the carbon. The charge–discharge profile in Fig. 5a for a C–Li cell shows significant irreversible capacity, which can be attributed to electrolyte decomposition and the possible formation of a solid electrolyte interface (SEI) film [20]. The carbon electrode delivers initial discharge capacity of 989.65, 726.98, and 619.77 mAh·g^{-1} at 0.1, 0.3, and 0.5 C. The initial discharge capacity is much higher than that of graphite (theoretical value 372 mAh·g^{-1}). What is more interesting is that subsequent cycles (Fig. 5b) show only a small capacity loss, which means stable charge–discharge performance. Moreover, under high current (0.5 C), cyclability is obviously better than at low current rate (0.1, 0.3 C), and cycle capacity efficiency reaches 99% at the 90th cycle. This phenomenon can be attributed to the

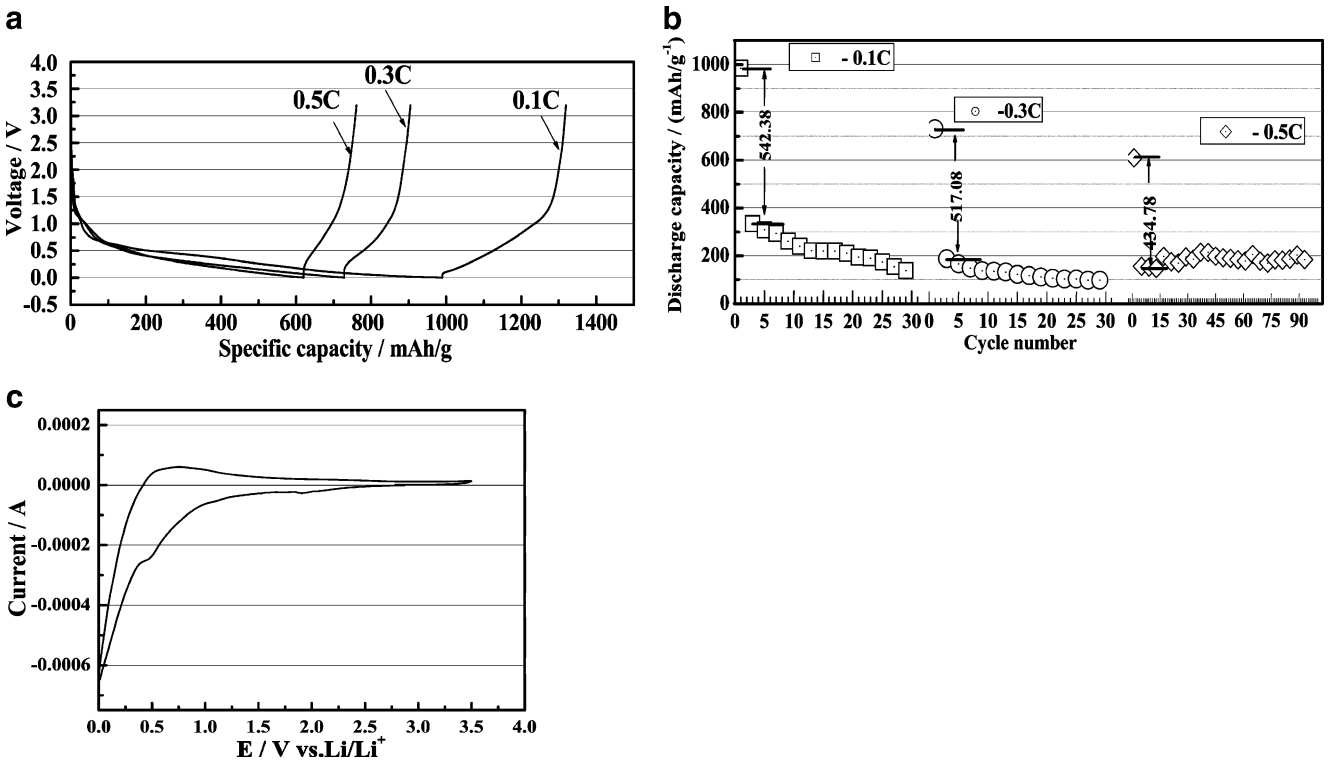

Fig. 5 **a** The first discharge–charge curves at 0.1, 0.3, and 0.5 C. **b** Cycle behaviors of C–Li cell at 0.1, 0.3, and 0.5 C. **c** Cycle voltammogram at 0.1 mV·s^{-1}

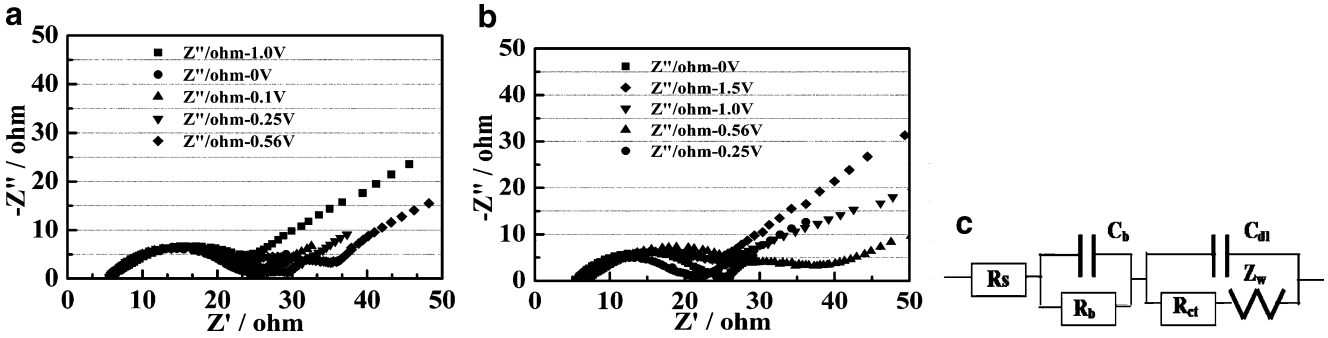

Fig. 6 Electrochemical impedance spectra of C–Li cell **a** during discharge, **b** during charge, and **c** equivalent circuit

special morphology, particle size, and surface functional groups of the carbon. In particular, the existence of various types of nitrogen confirmed by XPS may play a critical role in determining the reversible capacity. The higher electronegativity of nitrogen (3.5) than that of carbon (3.0) and the smaller diameter of nitrogen than that of carbon may lead to strong intercalation between carbon and lithium ion, and thus more lithium ion may be intercalated. At the same time, a significant amount of oxygen has been reported to increase cycling hysteresis [21]. It is possible that deposition of metallic lithium occurred, which may also contribute to deterioration of cycle performance.

To examine charge–discharge behavior, we examined a cyclic voltammogram for the C–Li cell at a scan rate of 0.1 $mV{\cdot}s^{-1}$ between 0 and 3.5 V, shown in Fig. 5c. The shape of the curve is similar to that reported in the literature [22], but the positions of anode and cathode peaks are different. This is a pair of single anodic and cathodic peaks, corresponding to intercalation–deintercalation of lithium into and from the carbon.

Electrochemical impedance spectroscopy was carried out to gain insight into the reason for the irreversible capacity. The spectrum was recorded at different voltages (vs. $Li–Li^+$; Fig. 6a, b). The voltage (vs. $Li–Li^+$) used in these measurements correspond to a region where it did not have Faraidaic contribution. During charge–discharge, the Nyquist plots gradually show two semicircles as the voltage is changed, indicating lithium-ion intercalation–deintercalation into or out of the carbon electrode. The Nyquist spectra were modeled using a Randles equivalent circuit, as is shown in Fig. 6c. The first semicircle, observed at high frequency, may be accounted for by the resistance of lithium-ion migration through the surface film (R_{sf}), i.e., SEI film, and corresponding capacitance, C_{sf}. The second semicircle in the middle-to-low frequency range may be ascribed to the charge transfer resistance, R_{ct}, and C_{dl}, the double-layer capacitance. Z_w is the Warburg impedance related to diffusion of lithium ion into bulk of the carbon electrode. R_s is the electrolyte resistance. As reported by Lery et al. [23], the main component in the outer part of the SEI is LiF, associated with a small amount of CH_3OCO_2Li and probably Li_2CO_3. The formation of SEI film is irreversible, but a dissolution–reprecipitation process for these species apparently occurs. Thus, SEI film formation associated with solvent decomposition results in significant irreversible capacity.

Electrochemical capacitive behavior of the carbon for supercapacitor

A significant presence of functional groups or complexes on the surface of carbon provides widespread possibilities for reversible chemisorption of active ions, which gives rise to extra capacitance [24]. Hence, the capacitive behavior of the carbon was investigated. The shape of a cyclic voltammogram (Fig. 7a) of the carbon electrode in 6-M

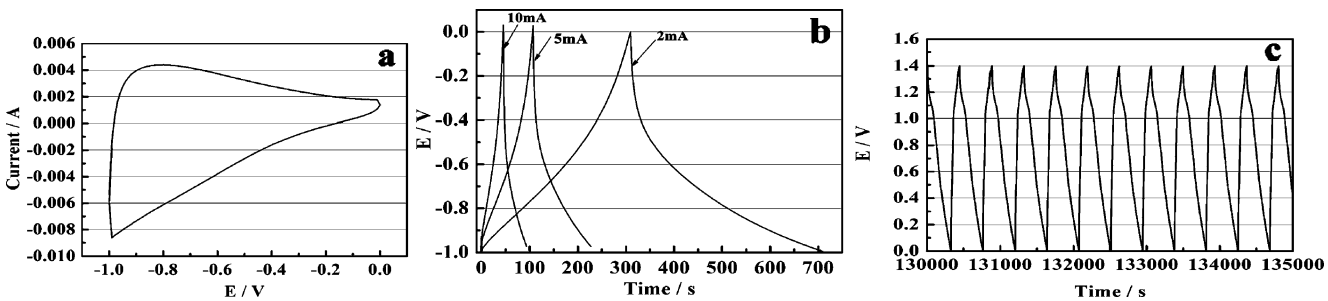

Fig. 7 Electrochemical capacitive characterization of the carbon **a** cycle voltammogram, at 5 $mV{\cdot}s^{-1}$; **b** charge–discharge, at 2, 5, and 10 mA; **c** charge–discharge of C–C symmetric capacitor at 2 mA

KOH solution is not rectangular, and a slight slop can be observed, which indicate some deviations from ideal double-layer capacitor behavior. The observed deviations can be attributed to a pseudo-capacitive contribution, which should be considered as a consequence of the presence of nitrogen incorporated in carbon. It was previously suggested that pyridinic nitrogen at the periphery of the graphene layers provides a pair of electrons, introducing electron donor properties to the layer [25]. The nitrogen species confirmed by XPS are located at accessible edges of the grapheme layers, and therefore they can easily contribute to total capacitance via a pseudo-capacitive effect [26]. It is also worth noting that current increases at the same time as potential shifts to more negative values, showing an increase in capacitance. This behavior was generally reported when KOH was used as the electrolyte [27].

Typical potential–time curves (Fig. 7b) of the carbon electrode were not the well-shaped triangles typical of ideal capacitive behavior. This result is in very good agreement with the cyclic voltammogram and may be ascribed to redox pseudo-capacitance affected by the ohmic resistance of the electrode. The specific capacitance of the carbon was calculated from galvanostatic discharge–charge at 2, 5, and 10 mA to be 120, 98, and 83 $F{\cdot}g^{-1}$. The capacitance is higher than that of an active carbon (110 $F{\cdot}g^{1}$) reported in literature [28]. However, oxygen-containing surface functional groups contribute a great deal of surface capacitance by holding more surface charge, and the existence of nitrogen also contributes to total capacitance via its pseudo-capacitive effect.

After the above experiments, a representative symmetrical supercapacitor was assembled, and a 2 mA galvanostatic discharge–charge test was conducted. As Fig. 7c shows, a good cycle performance was achieved with it, using the good pseudo-capacitive behavior resulted from the special physical and surface characteristics of the carbon.

Conclusions

The carbonization of a material containing beer yeast in argon produced a bead-like carbon, which consists of low graphitic and amorphous carbons with abundant surface functional groups. This carbon has the capability of lithium-ion intercalation–deintercalation. At 0.1 C, it showed an initial discharge capacity of 989.65 $mAh{\cdot}g^{-1}$, and good charge–discharge cycle performance was obtained, even at higher rates. Both the initial and reversible charge capacities are higher than that of other carbon, which may be attributed to the presence of surface functional groups. The presence of these oxygen- and nitrogen-containing groups gives the carbon effective capacitive behavior. These surface properties make the use of this carbon advantageous for energy storage and conversion systems. From an economic viewpoint, the carbonization of waste containing beer yeast may be considered as a promising route for producing a carbon with surface functions.

Acknowledgement This work was supported by Yangtze Normal University Research Start-up Foundation and Science and Technology Research Project of Chongqing Education Board (KJ081304).

References

1. Szymański GS, Zbigniew K, Biniak S, Świątkowski A (2002) Carbon 40:2627 doi:10.1016/S0008-6223(02)00188-4
2. Kim YJ, Lee HJ, Lee SW, Cho BW, Park CR (2005) Carbon 43:163 doi:10.1016/j.carbon.2004.09.001
3. Pittman CU Jr, He GR, Wu B, Gardner SD (1998) Carbon 36:25 doi:10.1016/S0008-6223(97)00147-4
4. Xie F, Phillips J, Silva IF, Palma MC, Menéndez JA (2000) Carbon 38:691 doi:10.1016/S0008-6223(99)00156-6
5. Hu CC, Wang CC (2004) J Power Sources 125:299 doi:10.1016/j.jpowsour.2003.08.002
6. Bagreev A, Angel Menendez J, Duhkno I, Tarasenko Y, Bandosz TJ (2004) Carbon 42:469 doi:10.1016/j.carbon.2003.10.042
7. Bonino F, Brutti S, Reale P, Scrosati B, Gherghel L, Wu J et al (2005) Adv Mater 17:743 doi:10.1002/adma.200401006
8. Inagaki M (2000) New carbons. Elsevier Science, Oxford
9. Su FB, Zhao XS, Wang Y, Zeng JH, Zhou ZC, Jim YL (2005) J Phys Chem B 109:20200 doi:10.1021/jp0541967
10. Wu YP, Fang SB, Jiang YY (1999) Solid State Ionics 120:117 doi:10.1016/S0167-2738(98)00158-1
11. Nakamura K, Fujitsuka M, Kitajima M (1990) Phys Rev B 41:12260 doi:10.1103/PhysRevB.41.12260
12. Deon H, Andrey B, Bandosz TJ (2004) Langmuir 20:3388 doi:10.1021/la0360613
13. Liu JW, Shao MW, Tang Q, Zhang SY, Qian YT (2003) J Phys Chem B 107:6329 doi:10.1021/jp034881i
14. Yang Q, Xu W, Tomita A, Kyotani T (2005) Chem Mater 17:2940 doi:10.1021/cm047830m
15. Lespade P, Al-jishi R, Dresselhaus MS (1982) Carbon 20:427 doi:10.1016/0008-6223(82)90043-4
16. Biniak S, Szymański G, Siedlewski J, Swiatkowski A (1997) Carbon 35:1799
17. Stańczyk K, Dziembaj R, Piwowarska Z, Witkowski S (1995) Carbon 33:1383 doi:10.1016/0008-6223(95)00084-Q
18. Darmstadt H, Roy C, Kaliaguine S (1994) Carbon 32:1399 doi:10.1016/0008-6223(94)90132-5
19. Figueiredo JL, Pereira MFR, Freitas MMA, Órfão JJM (1999) Carbon 37:1379 doi:10.1016/S0008-6223(98)00333-9
20. Flandrois S, Simon B (1999) Carbon 37:165 doi:10.1016/S0008-6223(98)00290-5
21. Frackowiak E, Gautier S, Gaucher H, Bonnamy S, Beguin F (1999) Carbon 37:61 doi:10.1016/S0008-6223(98)00187-0
22. Rahner D, Machill S, Schlorb H, Siury K, Kloss M, Plieth W (1998) J Solid State Electrochem 2:78 doi:10.1007/s100080050068

23. Lery S, Blanchard F, Dedryvere R, Martinez H, Carre B, Lemordant D et al (2005) Surf Interface Anal 37(10):773 doi:10.1002/sia.2072
24. Liu HT, He P, Li ZY, Liu Y, Li JH (2005) Electrochim Acta 51 (10):1925 doi:10.1016/j.electacta.2005.06.034
25. Koh M, Nakajima T (2000) Carbon 38(14):1947 doi:10.1016/S0008-6223(00)00040-3
26. Conway BE (1999) Electrochemical supercapacitor: scientific fundamentals and technological applications. Kluwer-Plenum, New York
27. Qu DY (2002) J Power Sources 109(2):403 doi:10.1016/S0378-7753(02)00108-8
28. Lufrano F, Staiti P, Minutoli M (2004) J Electrochem Soc 151 (1):64 doi:10.1149/1.1626670